Magnetoresistance and exchange bias in high Mn content melt-spun $Mn_{46}Ni_{42}Sn_{11}Sb_1$ alloy ribbon*

Qingxue Huang(黄庆学)[1,†], Fenghua Chen(陈峰华)[1,‡], Mingang Zhang(张敏刚)[1], and Xiaohong Xu(许小红)[2]

[1] *Heavy Machinery Engineering Research Center of Education Ministry, College of Mechanical Engineering, Taiyuan University of Science and Technology, Taiyuan* 030024, *China*

[2] *School of Chemistry and Materials Science, Key Laboratory of Magnetic Molecules and Magnetic Information Materials of Ministry of Education, Shanxi Normal University, Linfen* 041004, *China*

(Received 10 December 2015; revised manuscript received 25 January 2016; published online 5 April 2016)

Highly textured Heusler alloy $Mn_{46}Ni_{42}Sn_{11}Sb_1$ ribbons were prepared by melt spinning. The annealed high Mn content $Mn_{46}Ni_{42}Sn_{11}Sb_1$ ribbon cross-section microstructure, crystal structure, martensitic transformation (MT), and magnetoresistance (MR) properties were investigated. The MR in the annealed ribbon was assessed by the magnetic field direction perpendicular to the ribbon surface with the magnetic field up to 30 kOe. The large negative value of 25% for MR was obtained at 244 K. The exchange bias (EB) effects of the as-spun and annealed ribbons were investigated. After annealing, the EB effects have been improved by about 25 Oe at the temperature of 50 K. The magnetizations have increased approximately by 10% more than the as-spun ribbon.

Keywords: Heusler alloy, melt spun, magnetoresistance, exchange bias

PACS: 73.43.Qt **DOI:** 10.1088/1674-1056/25/5/057305

1. Introduction

The fact that the off-stoichiometric $Ni_2Mn_{1+x}X_{1-x}$ (X = In, Sb, or Sn) ferromagnetic shape memory alloys (FSMAs) undergo martensite transformation (MT) was reported by Sutou *et al.* for the first time.[1] Later, there were several research groups which studied the magnetic properties and magnetoresistance (MR) in both NiMnSn and NiMnIn alloys.[2–19] In 2006, giant MR (50%) was obtained in $Ni_{50}Mn_{34}In_{16}$ alloys in a magnetic field of 1 T,[2] while the $Ni_{50}Mn_{36}Sn_{14}$ got the same level (50%) in magnetic fields up to 17 T.[3] Even though a larger MR can be obtained in the NiMnIn than that in NiMnSn alloys, the necessity to the success of commercial use lies in the low-cost materials being available. By comparing the price of nickel and manganese, a high manganese content of alloy composition can effectively reduce the production cost.

Up to now, most of the research works have mainly focused on the $Ni_2Mn_{1+x}Sn_{1-x}$ alloys in which the content value of Mn is less than that of Ni,[4–8] and only a few reports are about high-Mn content Mn–Ni–Sn FSMAs.[9–14] Excessive Mn atoms occupy the vacant Sn sites, and their moments are coupled antiferromagnetically to those of the surrounding Mn atoms on the regular Mn sites.[9,11] It was pointed out that the MT temperatures in FSMAs were relative to the valence electron concentration e/at (electrons per atom).[3,11] The valence electron is determined as the number of 3d and 4s electrons of transition metals (Ni, Mn, Co, Fe, Cu, etc.) and the number of 5s and 5p electrons of In, Sn, or Sb. It is common knowledge that the coexistence of ferromagnetic (FM) and antiferromagnetic (AFM) phases in martensitic and the coupling at the AFM/FM interface would result in an exchange bias (EB) behavior in Ni–Mn based on FSMAs.[20,21] Researchers have reported the MCE changes in $Ni_{43}Mn_{46}Sn_{11-x}Sb_x$ and $Ni_{43}Mn_{46-x}Cu_xSn_{11}$ alloys at a low field.[22,23] As to the MR, exchange bias (EB) in these alloy ribbons are not well reported. Recently, some new research works suggest that the Mn-rich Heusler alloys such as Co_2MnAl, Mn_2CoAl, etc. have been found to present the possibility of high MR.[24–27]

Compared with the bulk material alloys, rapid quenching by melt spinning will provide a possibility to prepare a ribbon with a specific texture which could be favorable to MR and EB at a suitable magnetic field. In the present work, highly textured Heusler alloy $Mn_{46}Ni_{42}Sn_{11}Sb_1$ ribbons were prepared by melt spinning. The MR on textured $Mn_{46}Ni_{42}Sn_{11}Sb_1$ ribbons during the martensitic phase transitions were investigated. For a better understanding of the relationship among the magnetic field, magnetic resistance, and temperature, the isothermal MR-H was tested at the respective MT temperatures. EB behavior between as-spun and annealed ribbon is also studied.

*Project supported by the National Basic Research Program of China (Grant No. 2012CB722801), the Postdoctoral Science Foundation of China (Grant No. 2015M571285), the National Natural Science Foundation of China (Grant No. 51401140), the Postdoctoral Research Station Foundation of Taiyuan University of Science and Technology, China (Grant Nos. 20142014, 20152041, and 20151082), the Natural Science Foundation of Shanxi Province, China (Grants Nos. 2015021019, 2015091011, and 2015081011), and the Key Team of Scientific and Technological Innovation of Shanxi Province, China (Grant No. 2013131009).

†Corresponding author. E-mail: qxhuang_pd@163.com

‡Corresponding author. E-mail: phycfh@163.com

© 2016 Chinese Physical Society and IOP Publishing Ltd

2. Experimental

The ingot was induction melted in a quartz tube and melt-spun at a typical wheel surface speed of 10.0 m/s. The resulting ribbon was annealed at 1073 K for 1 h and cooled in the vacuum furnace. The average compositions of the ribbons were considered by the x-ray energy dispersive spectroscopy (EDS) analysis. The crystal structure of the sample was analyzed with a Panalytical X'Pert pro type x-ray diffractometer (XRD) with Cu Kα radiation. The lattice parameters were calculated through using Jade 5.0 XRD analytical software. The magnetic properties were measured using a multi-use vibrating sample magnetometer VersaLab system (Quantum Design), in a magnetic field up to 30 kOe. The temperature dependence of magnetization M–T curves was performed at a cooling/heating rate of 2 K/min. The electrical resistance was carried out by using a press contact assembly four-probe technique. The magnetic field direction was perpendicular to the free surface of the ribbon ($H_{\perp}$ the current). Resistance and MR were set as functions of the field (0 and 30 kOe) at different temperatures (150–300 K). Acquisition and control of the measurements were performed by using electrical transport option software (ETO, Quantum Design). Before the isothermal magnetic field MR curves were recorded, the sample was cooled down to the Curie temperature of the martensitic phase (T_C^M), and then heated to the measuring temperature in zero field. For the EB behavior test, the magnetic hysteresis loops (M–H) were used for as-spun and annealed ribbons at 50 K after cooling from 300 K in the present field of 5 kOe. The actual measurements were conducted from −4 kOe to 4 kOe.

3. Results and discussion

Typical SEM image of the fracture cross-section of the melt spun ribbon was presented in Fig. 1(a), showing a crystalline and columnar type microstructure. The average composition of the ribbons was by using the x-ray energy dispersive spectroscopy (EDS) analysis. The compositions were obtained based on five randomly made different points for the cross-section ribbon. The composition of the ribbon was considered to be $Mn_{46}Ni_{42}Sn_{11}Sb_1$ on average. The longer axis of the columnar grains has a tendency to align perpendicularly to the free surface of the ribbon, indicating that the rapid solidification process induces directional growth of textured polycrystalline ribbons. The ribbon thickness is about 40 μm. The fracture cross-section surfaces can be observed as well. Some tearing edges instead of typical brittle characteristics can be observed on the fracture surfaces. Lots of tearing edges provide the evidence that many courses were completed and a lot of energy was consumed before fracture.[16]

The XRD patterns of annealed ribbons measured at room temperature are presented in Fig. 1(b). It is clear that the sample crystal structure is in the cubic $L2_1$, as for the intensity ratio of $I_{(400)}/I_{(220)}$ is about 69.39%. From the XRD patterns, it is also established that ribbons exhibit crystallographic texture, which is in agreement with their grain-oriented columnar microstructure.[28,29] The crystal directions [400] are preferentially oriented perpendicular to the ribbon plane.[30] The lattice constant calculated from the XRD patterns is 5.984 Å for the annealed ribbon.

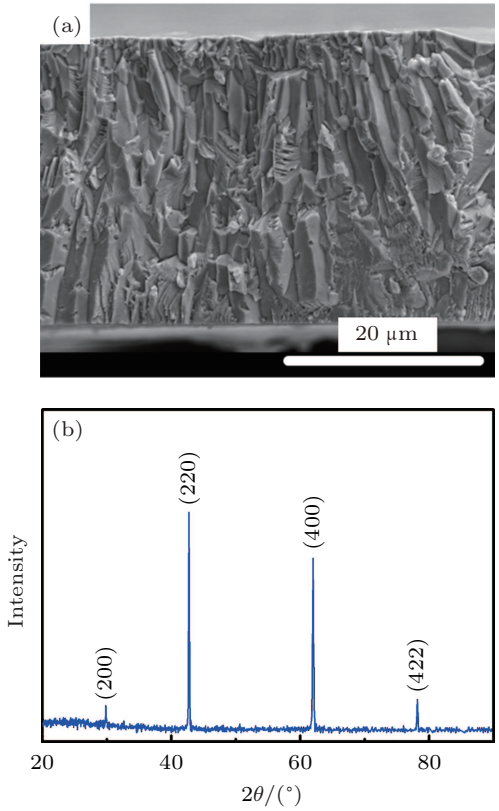


Fig. 1. (color online) The $Mn_{46}Ni_{42}Sn_{11}Sb_1$ alloy ribbons annealed at 1073 K for 1 h. (a) SEM micrograph of ribbon fractured cross section, and (b) the room-temperature XRD pattern.

The temperature dependence of the magnetization (M–T) curves and the temperature dependence of electrical resistance (R–T) for the $Mn_{46}Ni_{42}Sn_{11}Sb_1$ alloy ribbons were measured. Figure 2(a) shows the M–T curves for $Mn_{46}Ni_{42}Sn_{11}Sb_1$ on heating and cooling on a magnetic field of 100 Oe, respectively. As the M–T curves show, the thermal hysteresis is about 11 K around the MT temperature, which is attributed to the first-order structural transition. The first-order martensitic and austenitic start and finish at transition temperatures (M_s, M_f and A_s, A_f), respectively. The values of the M_s^M, M_f^M, A_s^M, and A_f^M estimated from the M–T curves, are determined to be 238, 229, 241, and 250 K, respectively. Figure 2(b) shows the R–T curves for the $Mn_{46}Ni_{42}Sn_{11}Sb_1$ alloy ribbons on heating and cooling without a magnetic field applied. The values of the M_s^R, M_f^R, A_s^R, and A_f^R, estimated from R–T curves, are determined to be 219, 236, 238, and 247 K, respectively. By comparing Fig. 2(a) with Fig. 2(b) of the first-order structural transformation procedure, the MT temperature estimated

from R–T on heating is about 3 K higher than that from M–T curves. The difference in MT temperature is caused by the texture ribbon with different dynamical driving factors, such as the testing theory, magnetic field directions, and magnetization experiments.

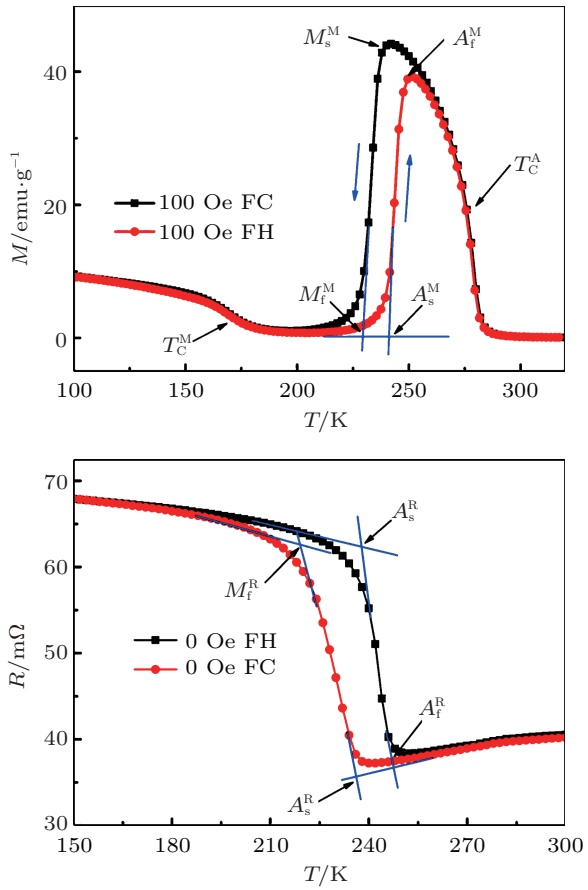


Fig. 2. (color online) The M–T curves for $Mn_{46}Ni_{42}Sn_{11}Sb_1$ alloy ribbons on heating and cooling under a magnetic field of 100 Oe (a), the R–T curves measured on heating and cooling without magnetic field (b).

The R–T curves for the $Mn_{46}Ni_{42}Sn_{11}Sb_1$ ribbons at 0 and 30 kOe on heating are plotted in Fig. 3(a). It is obvious that the MT temperature can be modified from changing the applied magnetic field. Under the magnetic field of 30 kOe, the MT temperature decreases by about 4 K for the ribbon, which results from the magnetic field shaping the transition temperature. Because the magnetic field can induce the MT in ferromagnetic shape memory alloys, this first-order transformation is often associated with a drastic change in resistance. Figure 3(b) displays the temperature dependence of MR for the ribbon. The MR is calculated using the formula $\mathrm{MR}(\%) = (R(H,T) - R(0,T))/R(0,T) \times 100\%$, where $R(H,T)$ and $R(0,T)$ are the resistance in the applied magnetic field and zero with the temperature, respectively. The large MR is only observed around the MT region, with a magnetic field of 30 kOe and a larger negative value of 25% for MR obtained. By comparing the result of $Ni_{44.1}Mn_{44.2}Sn_{11.7}$[17] with the magnetic fields at 30 kOe, their result only gets 10% MR at 268 K. While the $Ni_{50}Mn_{36}Sn_{14}$ gets 50% MR in a magnetic field up to 17 T.[3]

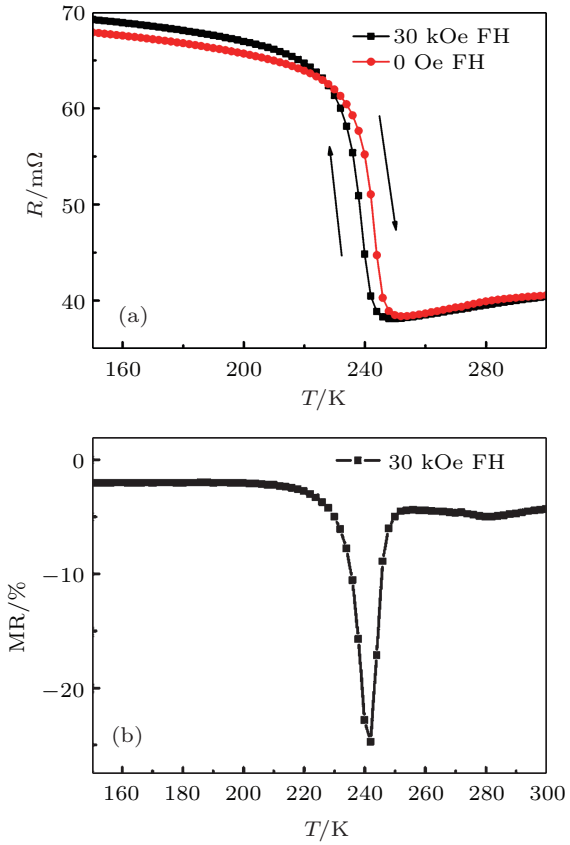


Fig. 3. (color online) (a) R–T curve at 0 and 30 kOe magnetic fields on heating. (b) MR as a function of temperature for $Mn_{46}Ni_{42}Sn_{11}Sb_1$ alloy ribbons on heating at 30 kOe.

As we already know, the large MR in these ribbons is likely to be caused by the field-induced change in electronic structure, which modifies the density of the states near the Fermi surface and leads to an abrupt change in resistance near the MT temperatures.[10,14]

In order to get a better understanding of the relationship among the magnetic field, magnetic resistance, and temperature, especially the relationship of the martensitic transformation processes, we tested the isothermal MR–H near the respective MT temperatures. In order to prevent austenite and martensitic phases in the sample from coexisting with each other, before the isothermal magnetic field MR–H curves were recorded, the sample was cooled down to T_C^M, and then warmed up after a 5-min waiting for consistency, monotonically without overshooting up to the target temperature in zero field at each step. Even though the isothermal MR–H near the MT temperatures has been well studied, each step increase 1 K is scarce.[12] Figure 4 shows the MR as a function of magnetic field at different constant temperatures for $Mn_{46}Ni_{42}Sn_{11}Sb_1$ alloy ribbons while MT was tested. In such case, with the applied magnetic field increasing, the magnetization changes could be essentially routed to domain walls

displacement or twin variants reorientation. However, we still get coexisting martensitic and austenite phases in the ribbon before 244 K, as shown in Fig. 4(a). Before the applied magnetic field increases, there is still a part of martensitic fraction (see Fig. 2(b)). From Fig. 4(a), we can see that at a 3-K temperature span (244–246 K), the highest MR at about 25% is obtained, and the MR remains almost constant. The fact that the MR increases with temperature before A_f^R means that the austenite phase has a larger MR than that of the martensitic phase. This can also be explained by the crystal structure lattice instability before the transformation was accomplished. Therefore, large MR can be ascribed to the field-induced MT temperatures decrease and the density of the states near the Fermi surface was modified. Resulting from the field-induced transition, the giant negative MR remains unchanged while the magnetic field decreases. On achieving the target temperatures before MT (see Fig. 4(a)), we get a coexisting martensite and austenite phases in the ribbon, in which there is a lot of fraction of martensite. At 245 K, the MR is about 11.5% of 10 kOe with the magnetic field increased, which was the same as 244 K. With the magnetic field increasing, a field-induced MT happens, the MR decreases with increasing magnetic field at magnetic fields from 10 to 17 kOe. In this case, with increasing the applied magnetic field, the magnetization changes could be essentially routed to domain walls displacement or twin variants reorientation. While the temperature increases to 246 K, the MR is only about 7.5% with the field up to 30 kOe, which means that the MT has been finished.

The isothermal M–H curves for the $Mn_{46}Ni_{42}Sn_{11}Sb_1$ alloy ribbon were measured at 241 K at a magnetic field up to 30 kOe. In Fig. 4(b), the typical magnetization curve at 241 K demonstrates the field-induced MT of the sample. Before the isothermal magnetic field MR curves were recorded, the sample was cooled down to the Curie temperature of the martensitic phase, and then heated to the measuring temperature in zero fields. As has been mentioned earlier, during the first-order structural transformation procedure, the MT temperature estimated from R–T is about 3 K higher than that at M–T curves at a magnetic field of 100 Oe. The magnetization jump in FSMAs would be attributed to two different interaction mechanisms. One mechanism may be the strong spin-phonon coupling. The other mechanism is due to the magnetic structure coupling on a microscopic scale between the magnetism and the martensitic variants, which leads to the magnetization jump near the MT. The metamagnetic characteristic in the M–H isotherms is associated with a field-induced reverse MT from a low magnetization martensitic state to a higher magnetization austenite state. On achieving the target temperatures before MT, we gain coexisting martensite and austenite phases in the ribbon, in which there is a high fraction of martensite. At 241 K, with the magnetic field increasing, a field-induced MT happens, and the magnetization increases with increasing magnetic field at a magnetic field from 10 to 17 kOe. In this case, with the applied magnetic field increasing, the magnetization changes could be essentially routed to domain walls displacement or twin variants reorientation. This phenomenon has been reported in magnetic field-induced MT in the other Ni–Mn based FSMAs.[13]

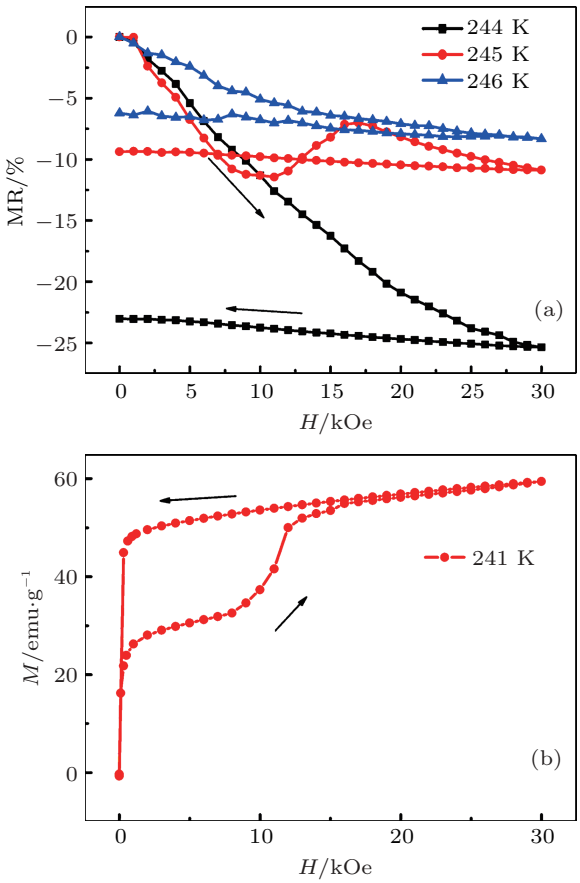


Fig. 4. (color online) The MR–H curves at different constant temperatures for $Mn_{46}Ni_{42}Sn_{11}Sb_1$ alloy ribbons (a). The typical isothermal M–H curves at constant temperatures (b). The sample was first cooled to 150 K and then heated back to the respective constant temperatures for MR measurement.

Figure 5 shows the M–H loops of the as-spun and annealed $Mn_{46}Ni_{42}Sn_{11}Sb_1$ ribbons measured at 50 K. The small variation of the Mn–Mn distance and the degree of atomic order can be affirmed in EB. A small but finite shift in the hysteresis loops was observed, which demonstrates the existence of EB in these ribbons. The values of EB field (H_E) and coercive field (H_C) were calculated by using $H_E = -(H_L + H_R)/2$ and $H_C = |H_L - H_R|/2$ (H_L and H_R are the left and right coercive fields, respectively). The H_E increases, while the H_C decreases for the annealed ribbon. The values of H_E are 90 and 115 Oe and H_C are 170 and 615 Oe, for the as-spun ribbon and annealed ribbons, respectively. Through comparing the EB result of high Mn content $Mn_{50}Ni_{40-x}Sn_{10+x}$ ($x = 0$, 0.5, and 1) alloys with the same temperature,[21] H_E and H_C are

determined to be 105 and 630, respectively. The ribbons have to undergo the structural relaxation and the growths of grain size in the annealing process, which will modify the degree of atomic order and form the ordered AFM/FM interface.[31,32] Therefore, the strengthening of the exchange coupling at the AFM/FM interface after the annealing would assume the responsibility of the increased H_E and the decreased H_C. While the heat treatment was performed, the magnetizations have increased by approximately 10% compared with the as-spun ribbon under the same applied magnetic field.

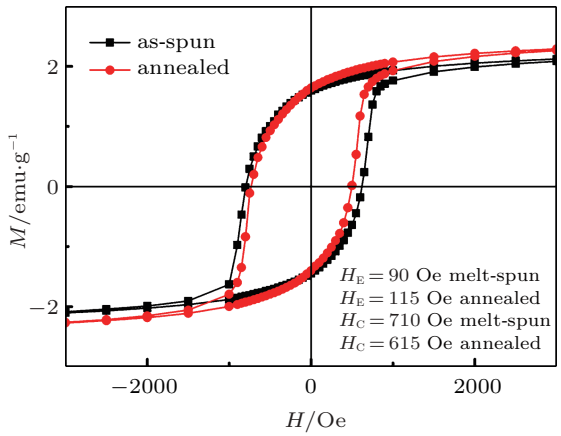


Fig. 5. (color online) The M–H loops of melt-spun and annealed $Mn_{46}Ni_{42}Sn_{11}Sb_1$ ribbons measured at 50 K.

4. Conclusion

Highly textured Heusler alloy $Mn_{46}Ni_{42}Sn_{11}Sb_1$ ribbons were prepared by melt spinning. The annealed high Mn content $Mn_{46}Ni_{42}Sn_{11}Sb_1$ ribbon prepared by melt-spun and cross-section microstructure, martensitic transformation (MT), and magnetoresistance (MR) properties were investigated. From the XRD patterns, it is clear that the sample crystal structure is in the cubic $L2_1$, and the intensity ratio of $I_{(400)}/I_{(220)}$ is about 69.39%. The ribbons exhibit that crystallographic texture is in agreement with their grain-oriented columnar microstructure. The crystal directions [400] are preferentially oriented perpendicular to the ribbon plane. The large negative value of 25% for MR is obtained at 244 K. At 245 K, a field-induced MT happens; we use the isothermal M–H curve to explain the reasons. The exchange bias (EB) effects of the as-spun and annealed ribbons were investigated. After annealing, the EB effects have been improved at the temperature of 50 K.

References

[1] Sutou Y, Imano Y, Koeda N, Omori T, Kainuma R, Ishida K and Oikawa K 2004 *Appl. Phys. Lett.* **85** 4358
[2] Sharma V K, Chattopadhyay M K, Shaeb K H B, Chouhan A and Roy S B 2006 *Appl. Phys. Lett.* **89** 222509
[3] Koyama K, Okada H, Watanabe K, Kanomata T, Kainuma R, Ito W, Oikawa K and Ishida K 2006 *Appl. Phys. Lett.* **89** 182510
[4] Chatterjee S, Giri S, Majumdar S and De S K 2008 *Phys. Rev. B* **77** 012404
[5] Wang B M, Wang L, Liu Y, Zhao B C, Zhao Y, Yang Y and Zhang H 2009 *J. Appl. Phys.* **106** 063909
[6] Dincer I, Yüzüak E and Elerman Y 2010 *J. Alloy. Compd.* **506** 508
[7] Pal D, Ghosh A and Mandal K 2014 *J. Magn. Magn. Mater.* **360** 183
[8] Banerjee A, Chaddah P, Dash S, Kumar K, Lakhani A, Chen X and Ramanujan R V 2011 *Phys. Rev. B* **84** 214420
[9] Sánchez Llamazares J L, Sanchez T, Santos J D, Pérez M J, Sanchez M L, Hernando, Escoda L, Suñol J J and Varga R 2008 *Appl. Phys. Lett.* **92** 012513
[10] Ghosh A and Mandal K 2013 *J. Phys. D: Appl. Phys.* **46** 435001
[11] Ma S C, Wang D H, Zhong Z C, Luo J M, Xu J L and Du Y W 2013 *Appl. Phys. Lett.* **102** 032407
[12] Khan M, Pathak A K, Paudel M R, Dubenko I, Stadler S and Ali N 2008 *J. Magn. Magn. Mater.* **320** L21
[13] Xuan H C, Zheng Y X, Ma S C, Cao Q Q, Wang D H and Du Y W 2010 *J. Appl. Phys.* **108** 103920
[14] Liu Z H, Wu Z G, Ma X Q, Wang W H, Liu Y and Wu G H 2011 *J. Appl. Phys.* **110** 013916
[15] Xuan H, Zhang Y, Li H, Han P, Wang D and Du Y W 2015 *Phys. Status Solidi A* **212** 1954
[16] Chen F H, Gong C W, Guo Y P, Zhang M G and Chai Y 2013 *Phys. Status Solidi A* **210** 2762
[17] Xuan H, Deng Y, Wang D, Zhang C, Han Z and Du Y 2008 *J. Phys. D: Appl. Phys.* **41** 215002
[18] Chen F H, Zhang M G, Chai Y S and Gong C W 2012 *Phys. Status Solidi A* **209** 1557
[19] Chen F H, Gong C W, Guo Y P, Zhang M G and Chai Y S 2014 *Chin. Phys. B* **23** 067501
[20] Esakki Muthu S, Rama Rao N V, Sridhara Rao D V, Manivel Raja M, Devarajan U and Arumugam S 2011 *J. Appl. Phys.* **110** 023904
[21] Xuan H C, Cao Q Q, Zhang C L, Ma S C, Chen S Y, Wang D H and Du Y W 2010 *Appl. Phys. Lett.* **96** 202502
[22] Wang D H, Zhang C L, Xuan H C, Han Z D, Zhang J R, Tang S L, Gu B X and Du Y W 2007 *J. Appl. Phys.* **102** 013909
[23] Xuan H C, Wang D H, Zhang C L, Han Z D, Liu H S, Gu B X and Du Y W 2007 *Solid State Commun.* **142** 591
[24] Kozina X, Karel J, Ouardi S, Chadov S, Fecher G H, Felser C, Stryganyuk G, Balke B, Ishikawa T, Uemura T, Yamamoto M, Ikenaga E, Ueda S and Kobayashi K 2014 *Phys. Rev. B* **89** 125116
[25] Feng Y, Tian C L, Yuan H K, Kuang A L and Chen H 2015 *J. Phys. D: Appl. Phys.* **48** 445003
[26] Feng Y, Zhou T, Chen X, Yuan H and Chen H 2015 *J. Magn. Magn. Mater.* **387** 118
[27] Feng Y, Zhou T, Chen X, Yuan H and Chen H 2015 *J. Phys. D: Appl. Phys.* **48** 285302
[28] Zhao X G, Tong M, Shih C W, Li B, Chang W C, Liu W and Zhang Z D 2013 *J. Appl. Phys.* **113** 17A913
[29] Wang W, Yu J, Zhai Q, Luo Z and Zheng H 2013 *Intermetallics* **42** 126
[30] Hernando B, Sánchez Llamazares J L, Prida V M, Baldomir D, Serantes D, Ilyn M and González J 2009 *Appl. Phys. Lett.* **94** 222502
[31] Ghosh A and Mandal K 2014 *Appl. Phys. Lett.* **104** 031905
[32] Zhao X G, Hsieh C C, Lai J H, Cheng X J, Chang W C, Cui W B, Liu W and Zhang Z D 2010 *Scripta Mater.* **63** 250